Optics Letters

Vibrational mid-infrared photothermal spectroscopy using a fiber laser probe: asymptotic limit in signal-to-baseline contrast

Atcha Totachawattana,[1,5] Hui Liu,[1,5] Alket Mertiri,[3,5] Mi K. Hong,[2,5] Shyamsunder Erramilli,[2,3,4,5] and Michelle Y. Sander[1,3,5,*]

[1]Department of Electrical and Computer Engineering, Boston University, 8 St. Mary's Street, Boston, Massachusetts 02115, USA
[2]Department of Physics, Boston University, 590 Commonwealth Avenue, Boston, Massachusetts 02115, USA
[3]Division of Materials Science and Engineering, Boston University, 15 St. Mary's Street, Brookline, Massachusetts 02446, USA
[4]Department of Biomedical Engineering, Boston University 44 Cummington Street, Boston, Massachusetts 02115, USA
[5]Photonics Center, Boston University, 8 St. Mary's Street, Boston, Massachusetts 02115, USA
*Corresponding author: msander@bu.edu

Received 2 November 2015; revised 25 November 2015; accepted 28 November 2015; posted 1 December 2015 (Doc. ID 251954); published 23 December 2015

We report on a mid-infrared photothermal spectroscopy system with a near-infrared fiber probe laser and a tunable quantum cascade pump laser. Photothermal spectra of a 6 μm-thick 4-octyl-4′-cyanobiphenyl liquid crystal sample are measured with a signal-to-baseline contrast above 10^3. As both the peak photothermal signal and the corresponding baseline increase linearly with probe power, the signal-to-baseline contrast converges to an asymptotic limit for a given pump power. This limit is independent of the probe power and characterizes the best contrast achievable for the system. This enables sensitive quantitative spectral characterization of linear infrared absorption features directly from photothermal spectroscopy measurements. © 2015 Optical Society of America

OCIS codes: (300.6430) Spectroscopy, photothermal; (190.4870) Photothermal effects; (300.6340) Spectroscopy, infrared; (300.6360) Spectroscopy, laser; (140.3510) Lasers, fiber; (140.3500) Lasers, erbium.

http://dx.doi.org/10.1364/OL.41.000179

Photothermal spectroscopy [1–3] has emerged as an attractive method for molecular bond-specific characterization of samples with nonradiative excited states. In photothermal spectroscopy, absorption at the pump laser wavelength induces thermal lensing effects that can be detected as phase changes in a probe laser. Sensitive photothermal spectroscopy with high contrast has been demonstrated at visible wavelengths for single molecule detection [4] and imaging of nanomaterials [5–7] and biological samples [8] such as heme proteins [9] and mitochondria in live cells [10,11]. With the development of tunable quantum cascade lasers (QCLs) [12,13], photothermal spectroscopy has been recently extended into the mid-infrared (mid-IR) [14–17].

Spectroscopy in the mid-IR is of particular interest due to the large number of characteristic vibrational and normal modes in what is known as the "fingerprint region" [18]. The high absorption cross-section of these vibrational modes (around 10^{10} times higher than the corresponding scattering cross-sections in conventional Raman spectroscopy) can be targeted for sensitive detection and characterization with high chemical specificity. This label-free and nondestructive technique has a range of applications, from chemical analysis [2] and biomedical diagnostics [19–21] to detection of hazardous materials [22,23].

The spectral brightness of tabletop QCL sources have been shown to exceed that of globar or thermal sources, often used in Fourier transform infrared spectroscopy (FTIR) and even synchrotron sources. This allows for high-contrast spectroscopy and imaging applications in the mid-IR [24]. Instead of a direct absorption measurement that relies on complex mid-IR detector technology, photothermal spectroscopy is performed in a pump-probe configuration. By choosing a probe laser wavelength in the visible or in the near-infrared (near-IR), commercially available optical detectors at room temperature with enhanced sensitivity can improve performance compared to mid-IR InSb and HgCdTe/MCT detectors, which in general require external cooling, e.g., in the form of cryogenic cooling.

Erbium-doped fiber lasers (EDFLs) operating in the near-IR present an attractive compact probe laser source whose wavelength is far removed from the strong mid-IR absorption bands. Fiber lasers offer robust performance operation, ease of alignment and reduced environmental sensitivity compared to free-space laser systems. Additionally, power scaling of the laser output power can be readily achieved by integrating erbium-doped fiber amplifiers (EDFAs), making it a versatile system in a compact footprint.

In this Letter, we present a mid-IR photothermal spectroscopy system that incorporates for the first time, to our knowledge, an EDFL as a probe laser. The signal-to-baseline

contrast evolution for increasing probe power values is characterized. Based on a linear increase of the photothermal signal and baseline with increasing probe powers, we derive an asymptotic limit for this ratio. For relatively low probe power values, a signal-to-baseline contrast above 93% of the asymptotic limit is obtained.

Our mid-IR photothermal system incorporates a custom-designed all-fiber laser probe together with a tunable QCL pump for label-free detection and spectral characterization. Absorption of the mid-IR pump beam induces a localized temperature profile in the sample. The pump-induced change in the refractive index results in a modulated forward scatter of the probe. The photothermal system is developed in a confocal geometry in transmission, where the pump and probe beam are focused onto the sample. The fiber probe beam is collimated into free space and collinearly combined with the free-space mid-IR pump beam at a dichroic mirror (DM) (see Fig. 1). The coaligned beams are focused onto the sample by a ZnSe objective (numerical aperture of 0.25, focal length of 6 mm). The QCL pump beam features a waist diameter of 20 μm and the near-IR probe, a waist diameter of 10 μm. As the lenses and the photodetector (PD) after the sample are designed for near-IR wavelengths, the probe beam is automatically filtered from the mid-IR pump beam. The transmitted probe beam is detected in an optical heterodyne configuration [16,25] in an amplified InGaAs PD (ET3000A, EOTech). A voltage-preamplifier (SR560, Stanford Research Systems, 50-times amplification between 10 kHz and 1 MHz in a low noise gain mode) together with a lock-in amplifier (HF2LI, Zurich Instruments) that is synchronized to the pump repetition rate selects the modulated photothermal signal of interest.

A pulsed QCL (model 41060, Daylight Solutions) serves as a tunable mid-IR pump laser (1575–1745 cm^{-1}) that is co-aligned with a cw EDFL operating in the near-IR. By tuning the QCL across selected characteristic vibrational absorption bands, photothermal spectra can be measured without the use of perturbing labels or any complex sample preparation. The QCL is pulsed at a repetition rate of 100 kHz and has a pulse duration of 500 ns, corresponding to a duty cycle of 5%. All experiments reported here are performed at a fixed QCL pump current, with an estimated pump power of 0.53 mW at the sample plane for a wavenumber of 1607 cm^{-1}, corresponding to a pump fluence of 8×10^{-4} J/cm^2 incident on the sample.

The EDFL has a maximum output power of 30 mW with 10% output coupling for 390 mW of coupled 976 nm pump power. The optical spectrum is centered at 1606 nm with a full width at half-maximum (FWHM) of 0.85 nm. For additional power scaling, the EDFL is amplified by two stages of home-built EDFA. After the first and second EDFA stages, the probe power is increased to 60 mW and 84 mW, respectively. For our experiments (Figs. 2 and 3) the probe power is adjusted using a mechanical attenuator.

For the photothermal studies, a 4-octyl-4′-cyanobiphenyl (8CB) liquid crystal sample with well-characterized and rich phase behavior [26–28] is chosen. The C-H scissoring band has a characteristic peak at 1607 cm^{-1} that is targeted in the following experiments. The 8CB liquid crystal is spaced between two 1-mm-thick CaF_2 windows with a 6-μm-thick mylar spacer. All measurements are performed at room temperature, where the liquid crystal sample is in the smectic-A phase. The photothermal spectrum is recorded at the lock-in output while the pump laser is scanned from 1580 to 1740 cm^{-1} in steps of 0.2 cm^{-1} at a fixed QCL pump current of 470 mA. For each probe power, three photothermal spectra are measured and fitted by a Gaussian curve with a constant offset as a function of wavenumber. In the following, the probe power shown corresponds to the near-IR optical power focused onto the sample. A constant offset is chosen to correspond to a zero-order polynomial fit over the wavenumber range from 1730 to 1740 cm^{-1}. This wavenumber range is defined as the baseline of the system, where the residual sample absorption is minimized. Figure 2 shows the Gaussian fit (lines) to the measured photothermal spectra (circles) at the indicated probe power values. As expected, the FWHM and center wavenumber of the Gaussian fits, 1606.23 ± 0.04 cm^{-1}, remain constant and are independent of probe power.

To evaluate the performance of the photothermal system, the signal-to-baseline contrast is analyzed. In this context, it is defined as the peak photothermal signal divided by the baseline (see Fig. 2). This provides a measure that effectively captures the spectroscopic contrast and allows for comparison to other spectroscopic methods.

For this Letter, the impact of probe power optimization for a fixed mid-IR QCL setting is studied. An optimized signal-to-baseline contrast is found at the given mid-IR pump power at the sample plane of 0.53 mW for a wavenumber of 1607 cm^{-1}. At higher pump powers, a nonlinear photothermal response

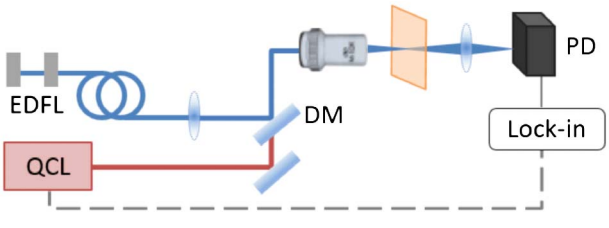

Fig. 1. Schematic of photothermal spectroscopy setup in transmission configuration. The QCL pump (mid-IR) and EDFL probe (near-IR) beams are collinearly combined in a dichroic mirror (DM) and focused onto the sample. The forward scatter of the probe beam is measured in a heterodyne detection scheme.

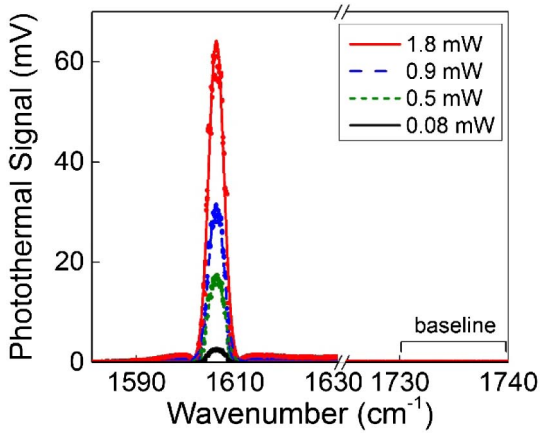

Fig. 2. Gaussian fits (lines) and measured photothermal spectra (circles) of 6 μm-thick 8CB liquid crystal for different probe power values incident on the sample. The wavenumber range from 1730–1740 cm^{-1} is chosen as a baseline.

can be observed (similar to [28]). Operating with a constant QCL power, the probe power focused on the sample is increased from 0.08 to 1.8 mW, an overall factor of ~23. The maximum photothermal signal from the amplitude of the Gaussian fit to the measured data is plotted in Fig. 3 (red dots). A weighted linear fit (red line) to the maximum photothermal signal with respect to increasing probe power is described by a slope $\alpha_s = 34.43$ mV/mW. The observed linear dependence of the photothermal signal ($S_{PT} \propto P_{pr}$) on the incident probe power (P_{pr}) follows directly from the analysis in [2,25,29,30]. Similarly, the baseline is evaluated for each corresponding probe power, as plotted in the inset in Fig. 3 (blue squares). The weighted linear fit (blue line) is characterized by a slope $\alpha_b = 0.026$ mV/mW. The standard error between the experimental peak photothermal signal to the Gaussian fit and between the baseline and the linear fit is indicated by error bars. For the maximum photothermal signal, the standard error is more than one order of magnitude smaller than the data values and thus hardly visible in Fig. 3. The non-zero y-intercept for both the photothermal signal and the baseline can be explained by the measurement background (amplified detector response when the pump laser is blocked with residual probe laser noise).

The lock-in amplifier detects the demodulated scattered power integrated over a solid angle determined by the collection optics and detector. The corresponding Green's function in the case of nanoparticle absorbers for linear photothermal spectroscopy have been published [25,29,31,32]. For an extended sample geometry with a homogeneous sample [2], as in our case, the probe beam scatter is determined by a convolution of the extended spatial distribution of the absorbers within the thermally modulated focus spot in the 8CB sample with the Green's function. For a beam waist diameter of 20 μm for the QCL and 10 μm for the fiber laser, absorbers within the probe beam focus distributed over the sample thickness of 6 μm will contribute to the photothermal signal (Rayleigh range of QCL beam ~50 μm). With a focused QCL mid-IR pump power of 0.53 mW at the sample, an upper limit for the temperature change within the 8CB layer is estimated at <1.5 K, assuming uniform attenuation within the sample. (The higher thermal conductivity of the surrounding CaF_2 windows can reduce the overall induced temperature rise, experimental measurements with a thermocouple indicated a temperature change on the order of 1 K). The scattering of the probe beam depends on the wavelength of the probe beam and the offset frequency Ω between the modulated probe signal and the unmodulated transmitted probe, which in this case is the repetition rate of the pump laser. Integrating the scattered power over the lock-in time constant leads to the measured photothermal signal. For both linear and nonlinear photothermal spectroscopy, the detected signal remains linear with probe power P_{pr}. Previously, in a photothermal imaging study [31], a linear dependence of the "noise" as a function of the number of frames averaged was shown. This effect was attributed to incomplete averaging when the exposure time was not an integer multiple of $2\pi/\Omega$ [31]. For our system, we expect a linear dependence as a function of power for both the signal ($= \alpha_s P_{pr} + \beta_s$) and the baseline ($= \alpha_b P_{pr} + \beta_b$), as shown in Fig. 3.

The measured signal-to-baseline contrast is calculated by dividing the maximum photothermal signal by the baseline value (see Fig. 3). Figure 4 shows the measured signal-to-baseline values (red circles) with respect to the probe power incident on the sample. Even at a low probe power of 0.08 mW (first measurement point), a signal-to-baseline contrast close to 300 is obtained. This value is increased by a factor of ~4 for a probe power value of 1.8 mW, with a high measured signal-to-baseline contrast of 1233 ± 32, underlining the good sensitivity of our system.

The ratio of the linear fits to the peak photothermal signal and baseline, described by $(\alpha_s P_{pr} + \beta_s)/(\alpha_b P_{pr} + \beta_b)$, is shown in Fig. 4 (solid red line). This indicates an asymptotic limit in the signal-to-baseline contrast of $\alpha_s/\alpha_b = 34.43/0.026 = 1324$ as the probe power approaches infinity. For the data shown, the experimental fit predicts the highest achievable signal-to-baseline contrast of this system to be 1324 (Fig. 4, black dashed line).

The highest experimentally measured signal-to-baseline contrast of 1233 ± 32 corresponds to over 93% of the

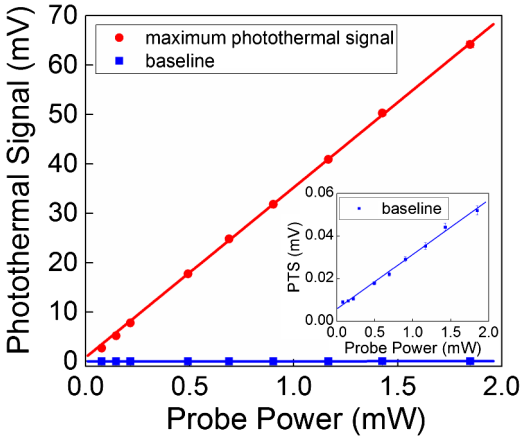

Fig. 3. Photothermal signal (PTS, red circles) and baseline (blue squares) as a function of probe power incident on the sample. The solid lines are weighted linear fits to the data. Inset: linear trend of the baseline (blue squares) with increasing probe power.

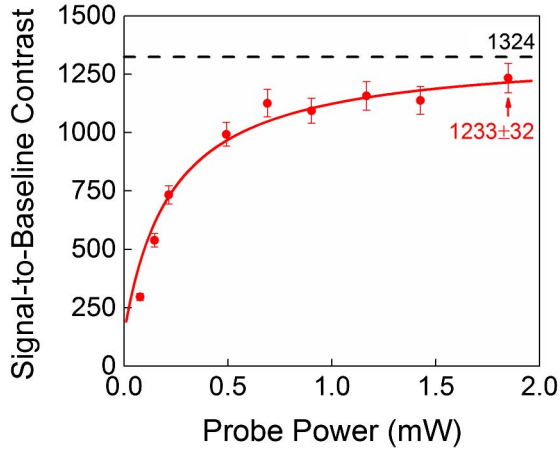

Fig. 4. Signal-to-baseline contrast (red circles) with error bars as a function of probe power incident on the sample. The solid red line shows the predicted signal-to-baseline contrast based on linear fits to the maximum photothermal signal and baseline from Fig. 3. A high signal-to-baseline contrast of 1233 ± 32 is measured. The black dashed line at 1324 represents the predicted asymptotic limit.

asymptotic limit of 1324. This indicates that optimized system performance can be achieved at relatively low probe powers incident onto the sample plane. Although the magnitude of both the photothermal signal and baseline will continue to increase with higher probe powers, the signal-to-baseline contrast will be capped. Based on the presented curve, a probe power of 4.8 mW is required to approach the asymptotic limit of 1324 within one standard error (±32). However, compared to the measured signal-to-baseline value of 1233 ± 32 at 1.8 mW, an increase by a factor of 2.7 in the probe power will only yield a signal-to-baseline ratio slightly below 98% of its asymptotic limit. Thus, the analysis of the measured and predicted signal-to-baseline curve demonstrates a "law of diminishing returns" in photothermal spectroscopy where above a certain probe power, further increase leads to diminished improvement in the signal-to-baseline contrast. The numerical values presented are specific for the mid-IR absorption spectra and the photothermal spectroscopy system presented. However, the principles are expected to hold in general for photothermal systems that exhibit linear trajectories for the peak photothermal signal and baseline with increasing probe power values. The physical significance of the asymptotic limit is that for a system where the residual absorption is the dominant contribution to the measured baseline, this limit describes the ratio between the extinction coefficients at the peak and the baseline of the sample. Thus, if the extinction coefficient for the baseline is known, a quantitative spectral characterization can be conducted independently from the specific experimental configuration and probe power.

For this 8CB sample, the corresponding transmission intensity ratio based on the absorbance measured from FTIR showed a good agreement with the determined photothermal asymptotic signal-to-baseline ratio. However, the FTIR measurements feature an order of magnitude larger measurement uncertainty compared to the presented photothermal method. In the asymptotic limit, a relatively small uncertainty is associated with the extracted absorption coefficients, due to the independence on probe power and on system implementation. This allows for quantitative measurements compared to other methods, where separate background measurements can contribute significant variations and systematic offsets. Thus, with the demonstrated photothermal spectroscopy method, quantitative spectral properties with the best possible contrast between the vibrational peak and baseline in the mid-IR spectrum can be determined.

To conclude, we presented a mid-IR photothermal spectroscopy system with a fiber laser probe in the near-IR that achieved signal-to-baseline values exceeding 10^3. Linear dependence of the photothermal signal of the C-H scissoring band in 8CB and the corresponding baseline with increasing probe power values leads to an asymptotic limit that is independent of probe power. For a probe power of 1.8 mW incident on the sample, a high signal-to-baseline contrast of 1233 ± 32 is measured, over 93% of the asymptotic limit of 1324. Further increase in the probe power results only in marginal improvements. This asymptotic limit is determined by the extinction coefficients at the peak and baseline absorption. We demonstrated that measurement of quantitative mid-IR absorption with high contrast is enabled with photothermal methods without the need for complex cryogenically cooled mid-IR detector technology.

Funding. College of Engineering, Boston University.

REFERENCES

1. M. E. Long, R. L. Swofford, and A. C. Albrecht, Science **191**, 183 (1976).
2. S. E. Bialkowski, *Photothermal Spectroscopy Methods for Chemical Analysis* (Wiley, 1996).
3. J. F. Power, Appl. Opt. **29**, 52 (1990).
4. A. Gaiduk, M. Yorulmaz, P. V. Ruijgrok, and M. Orrit, Science **330**, 353 (2010).
5. L. Cognet, C. Tardin, D. Boyer, D. Choquet, P. Tamarat, and B. Lounis, Proc. Natl. Acad. Sci. **100**, 11350 (2003).
6. P. Vermeulen, L. Cognet, and B. Lounis, J. Microsc. **254**, 115 (2014).
7. M. Yorulmaz, S. Nizzero, A. Hoggard, L.-Y. Wang, Y.-Y. Cai, M.-N. Su, W.-S. Chang, and S. Link, Nano Lett. **15**, 3041 (2015).
8. J. He, J. Miyazaki, N. Wang, H. Tsurui, and T. Kobayashi, Opt. Lett. **40**, 1141 (2015).
9. S. Lu, W. Min, S. Chong, G. R. Holtom, and X. S. Xie, Appl. Phys. Lett. **96**, 113701 (2010).
10. D. Lasne, G. A. Blab, F. De Giorgi, F. Ichas, B. Lounis, and L. Cognet, Opt Express **15**, 14184 (2007).
11. A. V. Brusnichkin, D. A. Nedosekin, E. I. Galanzha, Y. A. Vladimirov, E. F. Shevtsova, M. A. Proskurnin, and V. P. Zharov, J. Biophotonics **3**, 791 (2010).
12. J. Faist, F. Capasso, D. L. Sivco, C. Sirtori, A. L. Hutchinson, and A. Y. Cho, Science **264**, 553 (1994).
13. F. Capasso, C. Gmachl, R. Paiella, A. Tredicucci, A. L. Hutchinson, and A. Y. Cho, IEEE J. Sel. Top. Quantum Electron. **6**, 931 (2000).
14. M. Pfeifer, A. Ruf, and P. Fischer, Opt. Express **21**, 25643 (2013).
15. R. H. Farahi, A. Passian, L. Tetard, and T. Thundat, J. Phys. D. **45**, 125101 (2012).
16. A. Mërtiri, T. Jeys, V. Liberman, M. K. Hong, J. Mertz, H. Altug, and S. Erramilli, Appl. Phys. Lett. **101**, 4 (2012).
17. R. Furstenberg, C. A. Kendziora, M. R. Papantonakis, V. Nguyen, and R. A. McGill, Proc. SPIE **8374**, 837411 (2012).
18. P. R. G. Haseth and J. A. De, *Fourier Transform Infrared Spectrometry*, 2nd ed. (Wiley, 2007).
19. D. I. Ellis and R. Goodacre, Analyst **131**, 875 (2006).
20. D. C. Fernandez, R. Bhargava, S. M. Hewitt, and I. W. Levin, Nat. Biotechnol. **23**, 469 (2005).
21. C. H. Camp, Jr., Y. J. Lee, J. M. Heddleston, C. M. Hartshorn, A. R. H. Walker, J. N. Rich, J. D. Lathia, and M. T. Cicerone, Nat. Photonics **8**, 627 (2014).
22. C. A. K. R. Furstenberg, Appl. Phys. Lett. **93**, 224103 (2008).
23. P. M. Pellegrino, E. L. Holthoff, and M. E. Farrell, *Laser-Based Optical Detection of Explosives* (CRC Press, 2015).
24. K. Yeh, S. Kenkel, J.-N. Liu, and R. Bhargava, J. Anal. Chem. **87**, 485 (2015).
25. S. Berciaud, D. Lasne, G. A. Blab, L. Cognet, and B. Lounis, Phys. Rev. B **73**, 45424 (2006).
26. L. M. Babkov, I. I. Gnatyuk, and S. V. Trukhachev, J. Mol. Struct. **744-747**, 425 (2005).
27. M. Thomas and H. H. Richardson, Vib. Spectrosc. **24**, 137 (2000).
28. A. Mertiri, H. Altug, M. K. Hong, P. Mehta, J. Mertz, L. D. Ziegler, and S. Erramilli, ACS Photon. **1**, 696 (2014).
29. A. Gaiduk, P. V. Ruijgrok, M. Yorulmaz, and M. Orrit, Chem. Sci. **1**, 343 (2010).
30. J. Miyazaki, H. Tsurui, K. Kawasumi, and T. Kobayashi, Opt. Express **22**, 18833 (2014).
31. W. J. Eldridge, A. Meiri, A. Sheinfeld, M. T. Rinehart, and A. Wax, Biomed. Opt. Express **5**, 2517 (2014).
32. C. Pache, N. L. Bocchio, A. Bouwens, M. Villiger, C. Berclaz, J. Goulley, M. I. Gibson, C. Santschi, and T. Lasser, Opt. Express **20**, 21385 (2012).